Target loop antenna prototype with magnetic field reduction method

**Claude Daniel Assamoi[1], Yelakan Berenger Ouattara[1], Bi Tra Jean Claude Youan[1],
N'tcho Assoukpou Jean Gnamele[1], Vafi Doumbia[2]**
[1]Laboratory of Technology, University Félix Houphouët Boigny, Abidjan, Côte d'Ivoire
[2]Laboratory of Atmospheric Physics and Fluid Mechanics, University Félix Houphouët Boigny, Abidjan, Côte d'Ivoire

Article Info	ABSTRACT
	This paper proposes a new large loop antenna with a reduced magnetic field for a near field communication (NFC) target used in a metallic environment. It also defines a fairly clear method for controlling and, more specifically, reducing the magnetic field associated with loop antennas. This antenna consists of a circular winding, inside which we insert a square winding arranged in the shape of a diamond. The particular structure of this antenna shows that it is possible to dissociate the increase in the induced magnetic field, linked to its large size, from the increase in the number of windings. This is made possible by the application of the physical principle of overlapping magnetic fields, which results in partially destructive interference. *This is an open access article under the <u>CC BY-SA</u> license.*

Corresponding Author:

Claude Daniel Assamoi
Laboratory of Technology, University Félix Houphouët Boigny
01 BP V34 Abidjan 01, Cocody, Côte d'Ivoire
Email: assamoidaniel@gmail.com

1. INTRODUCTION

Near field communication (NFC) is a telecommunication technology inherited from radio frequency identification (RFID), and operating at frequency of 13.56 MHz [1], [2]. It is designed to operate over a theoretical distance of between 0 and 10 cm [3]. The essentials components are a target and an initiator, which communicate by inductive magnetic coupling thanks to loop antennae on each of them [4], [5]. These antennae are at the heart of the system's operation and their size or dimension is an important parameter in their choice, since some applications require small antennae, and others larger ones [6], [7]. The size of the antenna and the number of windings are therefore two factors to be taken into account when designing an NFC loop antenna, as electrical characteristics such as resistance and inductance increase as a function of these factors, which in turn impact on the antenna's performance [8]. In the specific case of large antennas, the known problems relate to the operating environment, the increase in resistance and inductance, because the latter is linked to the intensity of the induced magnetic field. This magnetic field must comply with the standards governing the NFC. To address the problem of increasing resistance, the authors in [9] propose an approach that consists of modifying the winding sequence of certain consecutive turns. This trick reduces the proximity effect between these consecutive windings and therefore the electrical resistance, despite the large size of the antenna and the number of windings. With regard to the operating environment, studies [10]–[13] show that metallic environments are very hostile to the operation of loop antennas. This environment reduces or completely cancels out the magnetic field induced in the windings. To strengthen the magnetic field, work has been carried out, often using ferrite as a magnetic barrier [14]. Lee *et al.* [15] proposed a standard rectangular antenna with five turns, with the fifth of

these acting as a parasitic Loop. Lee and Harackiewicz [16] proposed a rectangular antenna model with one winding. Zhu *et al.* [17] presented an approach based on the design of a hexagonal antenna with a non-uniform meander comprising six turns. However, all of these studies carried out to solve the problems listed above and relating to antenna large size does not provide enough information about the magnetic field intensity for some, or for others give results with magnetic field values beyond those published by the NFC standards. Whatever people may say, NFC standards like near field communication-interface and protocol 1 (NFC IP1) and near field communication-interface and protocol 2 (NFC IP2) exist, and it is important to design antennae that comply with the magnetic field values published in them [18], [19]. It is for this reason that we are proposing a new NFC loop antenna prototype for a target with large size, operating in a metallic environment, and having an induced magnetic field that meets the normative constraints as defined by the NFC standards. In addition to this new antenna prototype, we are defining a fairly clear way to reduce the magnetic field intensity for loop antennas. To complete this work, Firstly, we will define the methodology used to design and study the operation of the proposed new prototype antenna. We will then present the results obtained, shedding light on the physical phenomena that led to them. Finally, the results will be summarized in section 4.

2. METHOD

Figure 1 shows the overall structure under study. Firstly, it presents the new prototype antenna with all its components in Figure 1(a). Then, we indicate the simulation environment designed with high frequency structure simulator (HFSS) from Ansys electromagnetics suite 19.0 in Figure 1(b).
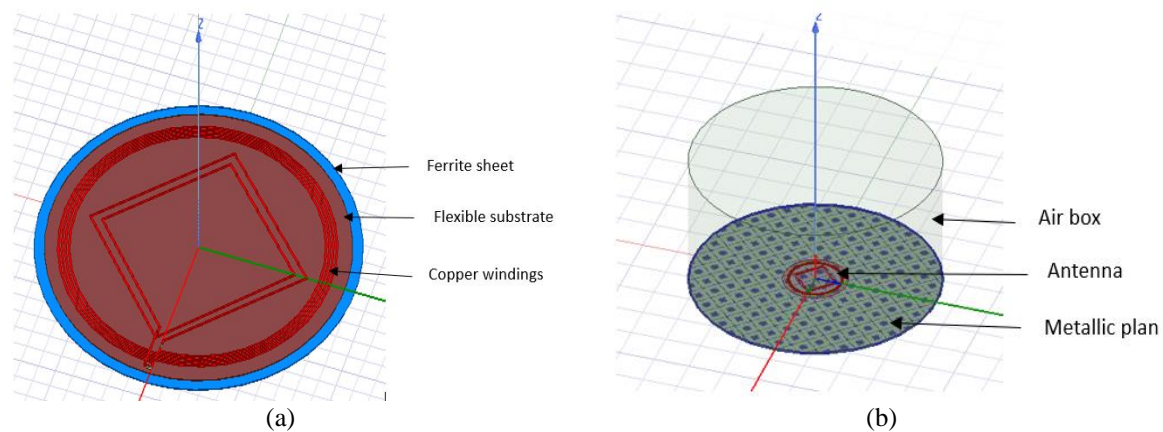

Figure 1. General view of system structure (a) mixed antenna 1 and (b) simulation environment

This antenna comprises copper windings printed on a flexible circular polyethylene substrate with a radius of $R_{substrate} = 41.3\ mm$ and a thickness of $e_{substrate} = 0.1\ mm$. The selection of copper was motivated by its exceptional electrical conductivity, and we use flexible materials, because it adheres well to a variety of surfaces [20], [21]. A thin ferrite sheet, with a thickness of $e_{ferrite} = 0.1\ mm$, is positioned beneath the substrate. This serves to separate the substrate from the metal, thereby protecting the antenna from the effects of eddy currents induced by the metal. The new prototype loop antenna combines two different geometric shapes in a single antenna. We have circular windings with two square windings inserted inside them in a diamond shape with respect to the antenna feed point. Characteristics such as the thickness and width of the windings are the same, while the gap between circular windings is different from that of the square windings. There is also a distance between the circular and square windings. These special provisions are intended to reduce the proximity effect, as required by the previous work reported, in order to avoid high resistance values. At the junction of the circular and square windings, an *RLC Lumped* port is inserted. This device represents the total capacitance of the antenna and the integrated circuit is added to it to achieve resonance.

Once all the antenna components have been designed, we need to set up the operating environment and analysis setup before moving on to the simulations. Figure 2 illustrates all the software configurations and settings that will enable us to put our antenna into almost real operating condition. All these settings and configurations are mainly made in the *Project Manager* window of the HFSS software in Figure 2(a).

The simulation environment is modeled using three essential functions. The *Perfect E* function (*perfE1*) is used to create the metallic environment and is applied to the ground plane below the substrate and ferrite (Boundaries > Assign > *Perfect E*). The antenna is excited using *the Lumped Port* function (*Excitation*), which is used to set the transmit power of the initiator to the target *(Excitation > Assign > Lumped Port)*. The last tool is the *Radiation* function (*Rad1*), which is applied to the air box surrounding the antenna. This air box constitutes the external environment in which the whole system is supposed to operate (*Boundaries > Assign > Radiation*). We finish by defining the analysis and simulation parameters. These parameters are set using the *Analysis* function. It is carried out in two phases, the first of which consists of defining the frequency at which the antenna structure is meshed, and the adaptive calculation process is carried out (*Setup1*) in Figure 2(b). This frequency is set at the operating frequency of the NFC. Here too, you can set the number of passes, which defines the accuracy of the results, and many other parameters. In the *General* tab, we choose the *Single* option for the frequency solution because our system operates at single frequency. In the second phase, we define a frequency range containing the NFC frequency (13.56 *Mhz*) for the solution calculations in Figure 2(c). After all these settings, we check the conformity of the entire system using the *Validate* function in Figure 2(d). The simulation is carried out using the *analysis* function and consists of varying the value of the capacitance symbolized by the *Lumped RLC (LumpedRLC1)* function to reach resonance using (1). Each time the capacitance is varied, we look at the variation curve of parameter S_{11} in order to check whether the system is operating at the frequency of 13.56 MHz. We repeat this process until we obtain a curve of the S_{11} parameter that resonates at 13.56 MHz. S_{11} represents how much power is reflected from the antenna, and hence is known as the reflection coefficient [22], [23].
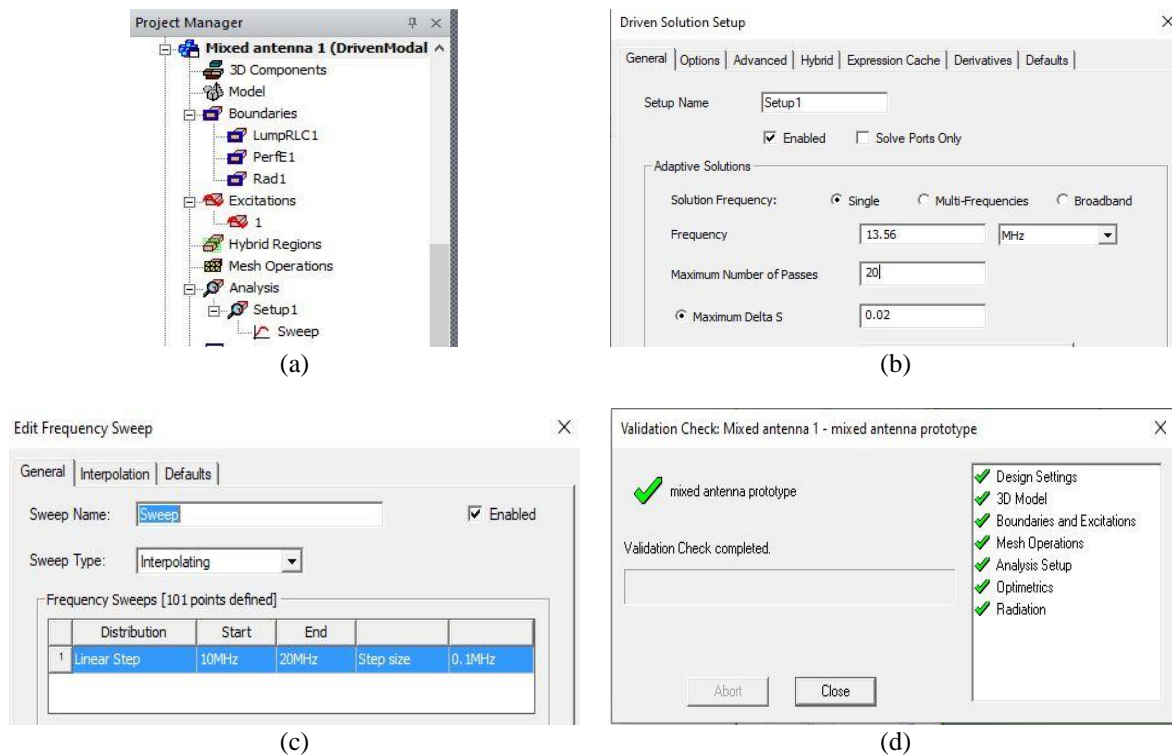

Figure 2. General view of experimental setup: (a) project manager settings window, (b) choice of operating frequency, (c) frequency interval for calculating solution, and (d) validation of design and various software settings

$$LCW_0^2 = 1 \tag{1}$$

From this resonance we can extract simulated parameters such as resistance, inductance and therefore the magnetic field curve evolution of the new prototype NFC loop antenna [24]. As we see, the only main tool that will be used throughout this work is the HFSS software, which is a powerful electromagnetic simulation tool. It will be used for the all designs, simulations and visualizations of all results [25], [26]. To

further refine our study, we designed the proposed new antenna prototype in three different models, which are a combination of a square and a circular antenna. We call these antennas respectively, mixed antenna 1, mixed antenna 2, mixed antenna 3 whose number of turns per antenna is as follows:
− Mixed antenna 1 (prototype 1): Four (04) windings for the circular antenna and two (02) windings for the square antenna.
− Mixed antenna 2 (prototype 2): Three (03) windings for the circular antenna and two (02) windings for the square antenna
− Mixed antenna 3 (prototype 3): Two (02) windings for the circular antenna and two (02) windings for the square antenna.
The characteristics of the circular and square turns of each model are given in Table 1.

Table 1. Characteristics of the new antenna prototype

Characteristics	C-W-4	C-W-3	C-W-2	S-W-2
Winding Radius max (mm)	37.5	36.5	35.5	-
Track Width (mm)	0.5	0.5	0.5	0.5
Track Thickness (mm)	0.035	0.035	0.035	0.035
Gap between tracks (mm)	0.5	0.5	0.5	2.7
Side of 1st turn (mm)	-	-	-	43.27
Side of 2nd turn (mm)	-	-	-	38.96

− C-W-4: Circular windings (4 turns)
− C-W-3: Circular windings (3 turns)
− C-W-2: Circular windings (2 turns)
− S-W-2: Square windings (2 turns)

To obtain the results on which we will base our discussions, the simulations will be carried out in two phases. The first phase will involve simulating the operation of our three new models. The second phase will involve simulating the operation of the circular and square components of the three models taken individually. In each phase we will extract, at resonance, the values of resistance, inductance and above all the magnetic field through its variation curve as a function of distance. These values will be discussed and compared to demonstrate the added value of our work.

3. RESULTS AND DISCUSSION
3.1. New prototype S_{11} parameter

First and foremost, we check whether the three models operate at the NFC frequency. This is done through the study of parameter S_{11}. Figure 3 shows the results obtained after simulations. The best resonance is obtained with prototype 1 (mixed antenna 1) with a more refined S_{11} parameter. The resonance frequency achieved for this model is more accurate with a good value, unlike the other models. This value is much closer to the desired 13.56 MHz.
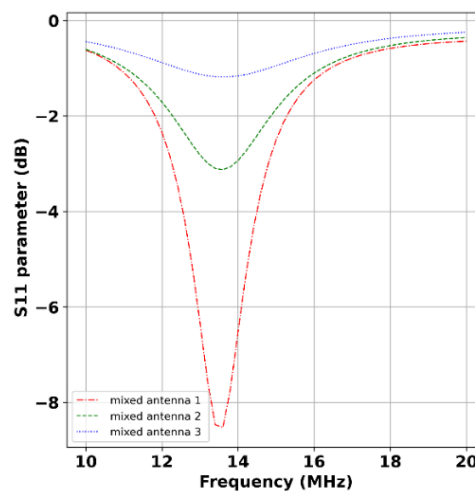

Figure 3. S_{11} parameter according to frequency for the three new models

Target loop antenna prototype with magnetic field reduction method (Claude Daniel Assamoi)

3.2. New prototype magnetic field

In order to gain a more comprehensive understanding of the outcomes of this research, we have conducted simulations with an excitation of 1 W. This value has been selected in order to encompass the majority of smartphones utilized as initiators within a real-world system. Indeed, some are equipped with the AS 39230 integrated circuit manufactured by AMS, providing smartphones with powerful initiators [27]. This choice is therefore a wise one.

Figure 4 illustrates the magnetic field results for each model of the new prototype and for the circular and square windings that comprise them. The magnetic field values for each model of the new prototype are less than those of the individual circular and square windings. Indeed, for the mixed antenna 1 in Figure 4(a), it can be observed that for the same given reading power emitted by the initiator represented by the excitation, the magnetic fields of the circular and square parts, when considered separately, are close to values of 23 A/m and 30 A/m, respectively.

In contrast, the magnetic field of the mixed antenna 1, composed of these same circular and square windings, is reduced and has a maximum value of $4.86\,A/m$. These results are consistent across mixed antenna 2 and 3 in Figures 4(b) and 4(c) respectively. Thus, the magnetic field values obtained for the three models are significantly lower than those of the circular and square antennas used to construct them. This reduction of the magnetic field value can be justified by a partially destructive interference between the initial magnetic field of the circular and square parts of the new prototype. Let's have a close look at the curves of these magnetic fields. Initially, the curve (the magnetic field) of the square antenna is above that of the circular antenna over distances of 0 to 12 mm for mixed antenna 1; 0 to 17 mm for mixed antenna 2; and 0 to 35 mm for mixed antenna 3.
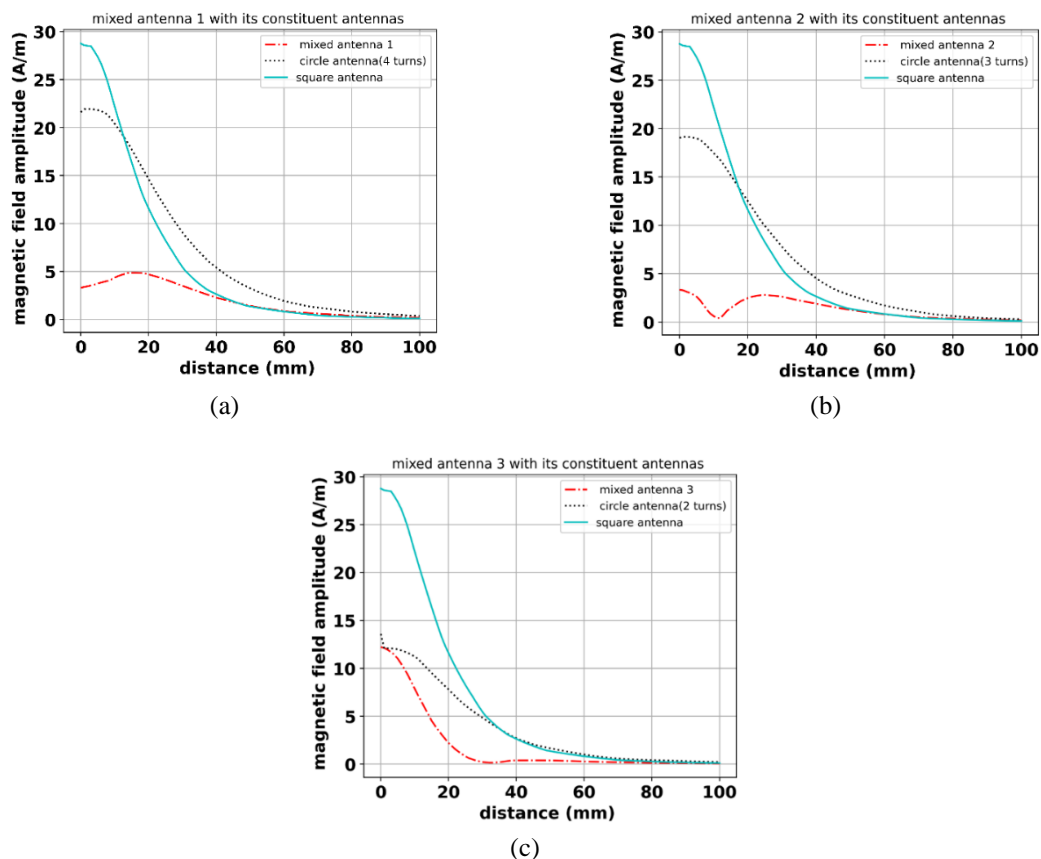

(a)

(b)

(c)

Figure 4. Comparing magnetic field (a) mixed antenna 1 and its constituent antennas; (b) mixed antenna 2 and its constituent antennas; and (c) mixed antenna 3 and his constituent antennas

The curves then overlap at a point just after these distances to finally see the curves of the circular's antennas above those of the square antenna. Meanwhile, physical theory defines interference as the result of two waves overlapping so that their displacements add up algebraically. If we apply this principle to our

initial circular and square magnetic fields, we can see that this overlap leads to a drop in the amplitude of the final magnetic field representing the magnetic field of the mixed antenna 1, mixed antenna 2 and mixed antenna 3 models. The application of this physical theory has therefore enabled us to design loop antennas large sizes with reduced magnetic field values. So, we can see that the new NFC loop antenna prototype for target that we are proposing does indeed make it possible to obtain reduced magnetic field values. In addition, with the good results obtained for the magnetic field, we also present the inductance and resistance values of our three models compare to their circular and square components as shown in Table 2.

We observe that the resistances of mixed antenna 2 (combination of three circular windings and two square windings) and mixed antenna 3 (combination of two circular windings and two square windings) with a larger number of turns (five and four respectively), have resistance values close to that of the circular windings of three and two windings taken separately. The resistance values increase slightly by 0.39 Ω and 0.28 Ω respectively despite the augmentation of the number of windings. On the other hand, the resistance value of mixed antenna 1 (combination of four circular windings and two square windings) is 22.8 Ω compared with the resistance value of the 4-turn circular windings, which is 35 Ω. The principle of reducing the proximity effect is therefore respected for our three models of the new prototype. With regard to the inductances of the three models also, we can logically see a considerable increase in these due to an increase in the number of turns. But the striking fact here and which is the focus of our work is that the overall values of the magnetic field of our three models remain relatively lower as mentioned earlier in this same section despite the high values of inductances. Also, to better appreciate the phenomenon of interference due to the overlapping of two magnetic fields, which results in the reduction of the final magnetic field of the new prototype, we can observe the surface current distributions. As in the case of the magnetic field, we will see how the surface current distribution of the circular and square components of the new prototype interacts.

Table 2. Simulated values of resistance and inductance

Antenna prototype	Resistance (Ω)	Inductance (μH)	Magnetic field maximum value (*A/m*)
Mixed antenna 1	22.8	21.06	4.86
Mixed antenna 2	8.9	4.2	3.32
Mixed antenna 3	3.39	1.92	12.21
Circular antenna (4-turns)	35	6.26	21.93
Circular antenna (3-turns)	8.51	2.9	19.15
Circular antenna (2-turns)	3.11	1.08	13.6
Square antenna (2-turns)	1.87	0.62	28.76

3.3. New prototype surface current density

In this section, we will look at the surface current distribution around the windings of our three new models. More precisely, we will see how the surface current distribution specific to each format composing the new model interacts to form the new prototype's antenna surface current distribution. To do this, we set the same minimum and maximum values of the surface current for each case and observe how this current is distributed over the whole substrate. The result of this interaction of the surface currents will situate us on the evolution of the global magnetic field of these new models since the final objective is to reduce it. For each case, we will present side by side the distribution of the surface current of each format taken separately and that of the new prototype resulting from their association.

3.3.1. Mixed antenna 1

For this first case study, we show the all-surfaces currents densities in Figure 5. More distinctively, we have the areal current densities of the square and circular components in Figures 5(a) and 5(b) respectively. The mixed antenna 1 model surface current density is shown in Figure 5(c). The surface current density of the four turns circular antenna is stronger around the windings and weaker around the center of the antenna and in some detached zones. This density is less compact in these areas of low concentration. In contrast, the square 2-turn antenna has a high surface current density that is almost uniformly distributed over the entire surface of the antenna. There are just a few small areas of low density on the outside of the windings. This analysis for the square antenna remains valid for the other two mixed antenna models 2 and 3, since they are partly formed by this same antenna. By combining these two formats to form the mixed antenna 1 model, we can distinguish two particular zones. At the center of the antenna, we see a lower surface current density, which is more compact this time, with a larger surface area. The areas of highest concentration are located a little closer to the windings and are interspersed with a slightly greater number of areas of low surface current density. It is therefore clear that the surface current densities of the two square and four circular windings have merged and interacted when combined to form the mixed antenna 1 model.

The large number of areas of low areal current density and the compactness of the largest area indicate their strong interaction, leading to reducing considerably the final magnetic field.
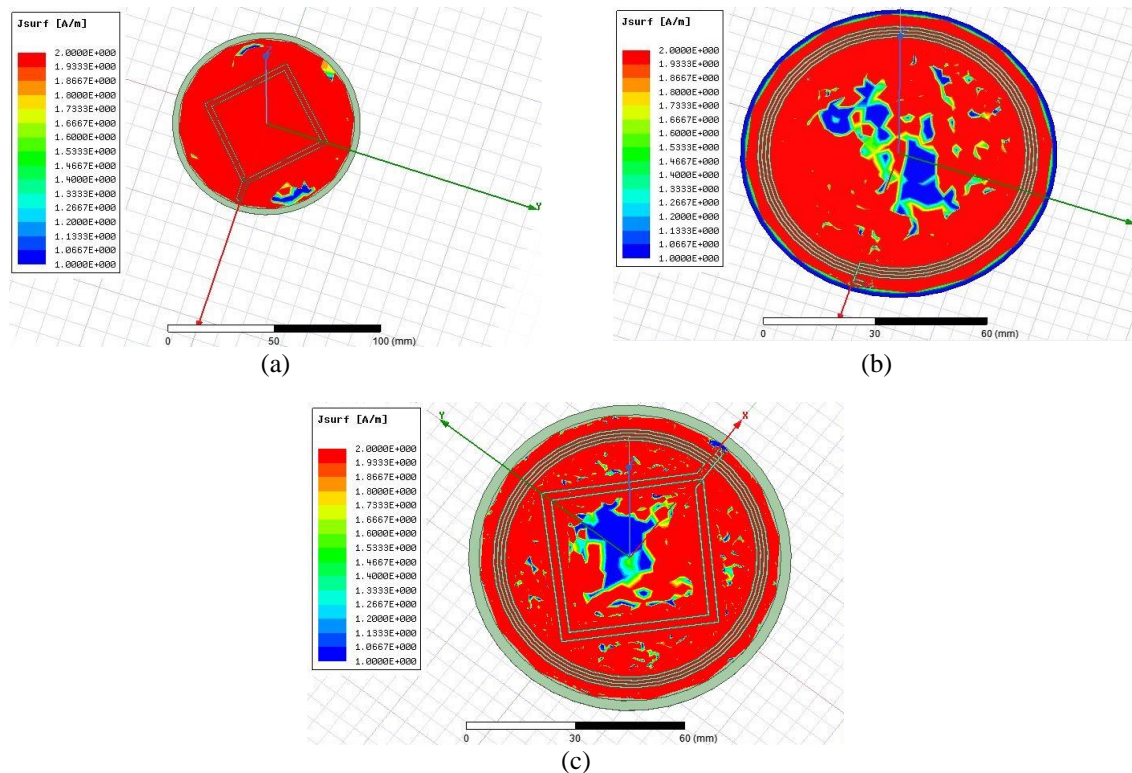

(a) (b)

(c)

Figure 5. Formation of the surface current density (a) two turns square antenna; (b) four turns circular antenna surface current; and (c) mixed antenna 1

3.3.2. Mixed antenna 2

Figure 6 shows the formation of surface current density for the second case study. More specifically, the surface current densities of the two-turns square and three-turns circular components are shown in Figure 6(a) and Figure 6(b) respectively. The surface current density resulting from their combination to form the mixed antenna 2 model is shown in Figure 6(c).

The reduction in the area of low surface current density for the mixed antenna 2 model demonstrates the strong interaction between the two initial surface currents of the square and circular windings. Initially, the circular antenna had a larger low-density zone, and its combination with the square windings has further reduced these low-density zones, which are spread throughout the mixed antenna 2 area.

3.3.3. Mixed antenna 3

Figure 7 shows the formation of surface current density for the last case study. Figure 7(c) shows the surface current density of the mixed antenna 3 model. Those of its two turns square and two turns circular components are shown in Figures 7(a) and 7(b) respectively. We can see from the surface current mapping that the mixed antenna 3 model has several small areas of low surface current density, the most important of which are located in the middle of the antenna. These low-density zones are more numerous than the initial circular and square windings. This justifies low interaction and therefore lower destructive interference compared with the mixed antenna 1 and mixed antenna 2 models.

Finally, the study of the areal current density distribution gives results that guide us on the evolution of the final magnetic field of each model of the new prototype. Indeed, due to the high or low level of interactions, we can affirm that a destructive interference occurs, allowing a decrease of the final magnetic field. The conclusive results of this section demonstrate once again the relevance of our method of reducing the magnetic field associated with the particular structure of the mixed antenna 1, mixed antenna 2 and mixed antenna 3 models.
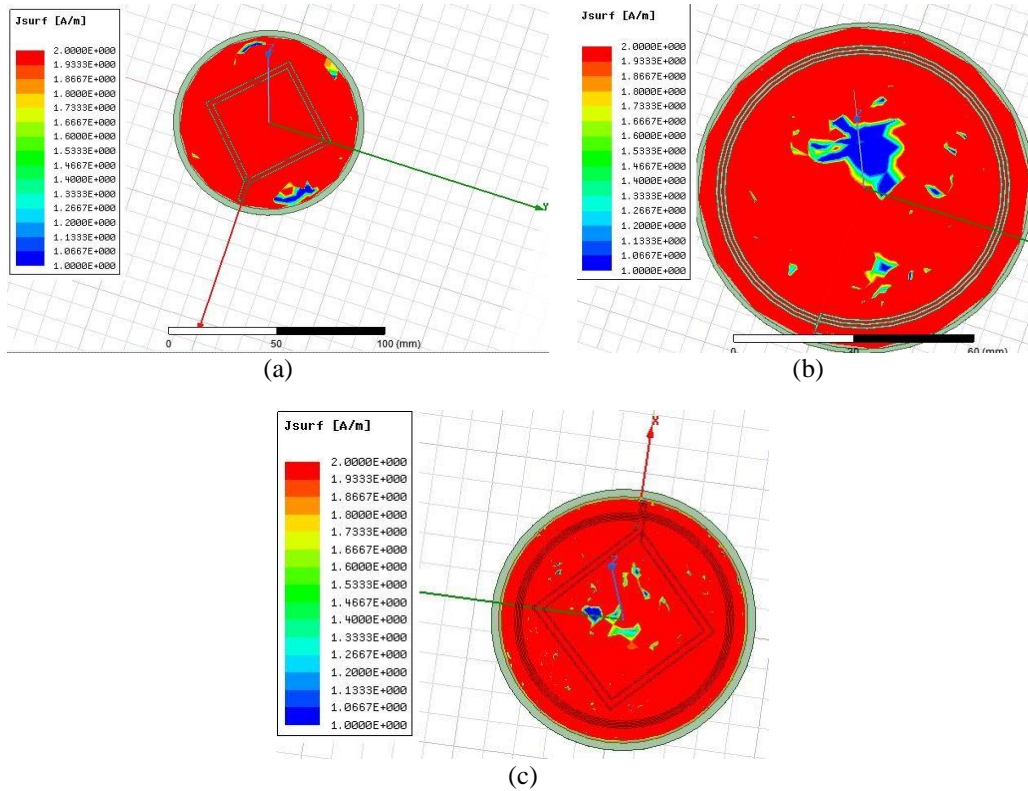
(a)

(b)

(c)

Figure 6. Formation of the surface current density (a) two turns square antenna; (b) three turns circular antenna; and (c) mixed antenna 2
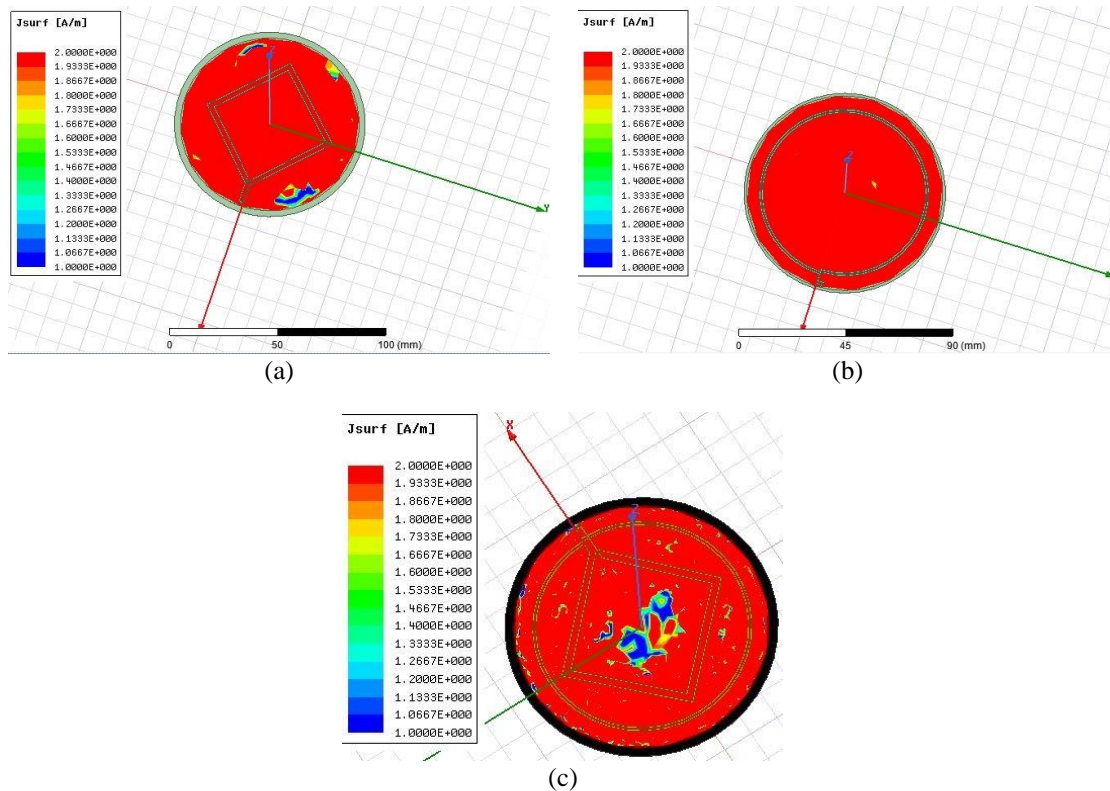

(a)

(b)

(c)

Figure 7. formation of the surface current density (a) two turns square antenna; (b) two turns circular antenna; and (c) mixed antenna 2

3.4. Comparison with previous studies

Table 3 summarizes the studies on large antennas. These studies were carried out either to investigate large standard antennas or to provide solutions to the operating difficulties mentioned in the introduction by means of new NFC antenna structures. This table will be used as a comparative basis to better elucidate the good results we are obtaining with our new antenna prototype.

Table 3. Comparative table of magnetic field

Reference	Antenna size (mm²)	Number of turns	Maximum magnetic field (A/m)
[8]	50×50	6	No information
[9]	45×55	5	No information
[15]	45×55	5	[10, 16]
[16]	46×8	1	≥ 20
[17]	38.6×46	6	No information

It can be observed that the maximum values of magnetic field proposed in [15] are between 10 A/m and 16 A/m for the proposed new antenna structure. In contrast, the maximum magnetic field values achieved in [16] are above 20 A/m. the other works in this table do not provide clear information on the possible magnetic field intensity obtained. A comparison with the maximum magnetic field values of the three models reveals that only the mixed antenna 3 model exhibits a slightly higher magnetic field value than those reported in studies proposing a new NFC antenna structure as shown in Table 2 compared to Table 3. With regard to the models mixed antennas 1 and 2, their maximum magnetic field values are below those obtained in previous studies proposed in Table 3. Based on the available data, it can be observed that the combined approach of the association of circular and square windings to form a new loop antenna is capable to induce magnetic fields that comply with the standards values despite their large dimensions. Initially, we were able to reduce the magnetic field for a large antenna with an equivalent or greater number of windings compared to the new antenna structures developed in previous studies in Table 3.

However, these magnetic field values must be standardized in order to comply with the imposed NFC standards, and to achieve the desired characteristics. Referring to Table 2 and Figure 8, it can be observed that only the mixed antenna models 1 and 2 have magnetic field values below the standard values. In order to conclude this section, it is necessary to consider the maximum reading capabilities of the antennas that have been designed. If we base our calculations on the admissible magnetic field values for the largest antenna size permitted by the standard, we can demonstrate the reading ranges of our three models in relation to the experimental conditions, as previously outlined in the methodology section. In reference to Figure 8, and the magnetic field values prescribed by the standard, the regulatory distance intervals for each model are as follows: $[0\ mm; 49\ mm]$ (mixed antenna 1); $[0\ mm; 7\ mm] \cup [16\ mm; 45\ mm]$ (mixed antenna 2).

The mixed antenna 3 model, which has a magnetic field strength exceeding the standard, is not considered. The only model that complies with the standard is the mixed antenna 1 model. This model delivers a magnetic field strength that is within the standard limits over the entire distance range from 0 to $49\ mm$ as shown in Figure 8. The mixed antenna 1 model thus appears to offer considerable potential for use in metallic environments, given its inductance, magnetic field induction, resistance and detection range characteristics.
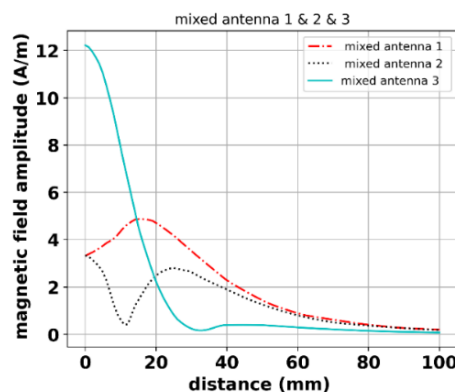

Figure 8. Mixed antenna 1-2-3 magnetic field

4.   CONCLUSION

A new prototype large loop NFC antenna has been proposed for the target, combining circular and square windings to reduce the magnetic field strength. The proposed antenna was designed with a ferrite foil to protect it from the effects of metal. After comparison with previous studies and standard antennas, we have seen that this large antenna induces magnetic field values that comply with NFC standards and also offers a good detection range. These results were made possible by a particular dimensioning and layout of the circular and square components of the new antenna prototype, resulting in an overlap between the initial magnetic fields of its components. This overlap is at the origin of the interference that has caused this reduction in the magnetic field, according to a well-known physical principle. The mixed antenna 1 model, consisting of a square antenna with two windings and a circular antenna with four windings, appears to be the best prototype in terms of desired efficiency, dimensions, magnetic field values and reading range in compliance with NFC standards. This antenna design technique for reducing magnetic field values offers a solution in applications requiring large antennas and where it is necessary to maintain low magnetic field levels to reduce possible electromagnetic incompatibilities.

REFERENCES

[1]   S. Kolev, "Designing a NFC system," in *2021 56th International Scientific Conference on Information, Communication and Energy Systems and Technologies (ICEST)*, Jun. 2021, pp. 111–113, doi: 10.1109/ICEST52640.2021.9483482.

[2]   M. A. Ali Khan, M. Hanif Ali, A. K. Fazlul Haque, C. Debnath, and S. K. Bhowmik, "An efficient and optimized tracking framework through optimizing algorithm in a deep forest using NFC," *Indonesian Journal of Electrical Engineering and Computer Science*, vol. 19, no. 2, pp. 884–889, Aug. 2020, doi: 10.11591/ijeecs.v19.i2.pp884-889.

[3]   A. R and V. D. Shastrimat V, "Qualitative assessment on effectiveness of security approaches towards safeguarding NFC devices services," *International Journal of Electrical and Computer Engineering*, vol. 8, no. 2, pp. 1214-1221, Apr. 2018, doi: 10.11591/ijece.v8i2.pp1214-1221.

[4]   C. Degen, "Inductive coupling for wireless power transfer and near-field communication," *EURASIP Journal on Wireless Communications and Networking*, vol. 2021, no. 1, Dec. 2021, doi: 10.1186/s13638-021-01994-4.

[5]   S. A. Mitilineos *et al.*, "A wearable NFC antenna sewn on leather substrate for immersive IoT applications," *Textile & Leather Review*, vol. 5, pp. 70–84, Feb. 2022, doi: 10.31881/TLR.2022.03.

[6]   J. Kim *et al.*, "Miniaturized flexible electronic systems with wireless power and near-field communication capabilities," *Advanced Functional Materials*, vol. 25, no. 30, pp. 4761–4767, Aug. 2015, doi: 10.1002/adfm.201501590.

[7]   M. H. Misran, S. K. Abdul Rahim, M. A. Meor Said, and M. A. Othman, "A systematic optimization procedure of antenna miniaturization for efficient wireless energy transfer," *International Journal of Electrical and Computer Engineering*, vol. 9, no. 4, pp. 3159–3166, Aug. 2019, doi: 10.11591/ijece.v9i4.pp3159-3166.

[8]   N. Mohd Faudzi *et al.*, "Analysis of flexible silver-printed NFC tag antenna on miniaturization and bending effect," *ESTEEM Academic Journal*, vol. 19, no. March, pp. 54–67, Mar. 2023, doi: 10.24191/esteem.v19iMarch.21262.

[9]   B. Lee, B. Kim, F. J. Harackiewicz, B. Mun, and H. Lee, "NFC antenna design for low-permeability ferromagnetic material," *IEEE Antennas and Wireless Propagation Letters*, vol. 13, pp. 59–62, 2014, doi: 10.1109/LAWP.2013.2296307.

[10]   S. S. Lau, "Practical design of 13.56MHz near field communication (NFC) and radio frequency identification (RFID) antenna using ferrite sheet on metallic surface by network analyzer," in *2015 IEEE International Conference on Industrial Engineering and Engineering Management (IEEM)*, Dec. 2015, pp. 1362–1366, doi: 10.1109/IEEM.2015.7385870.

[11]   Y. Nakagawa, N. Michishita, and H. Morishita, "A study on antenna with characteristics of insensitive to metal for installation in proximity to two metal walls," *Journal of Advanced Simulation in Science and Engineering*, vol. 6, no. 1, pp. 118–127, 2019, doi: 10.15748/jasse.6.118.

[12]   J. Victoria *et al.*, "Study of a novel high permeability ferrite sheet intended for near field communication systems," in *2019 IEEE International Symposium on Electromagnetic Compatibility, Signal & Power Integrity (EMC+SIPI)*, Jul. 2019, pp. 78–83, doi: 10.1109/ISEMC.2019.8825260.

[13]   N. O. Romero-Arismendi, J. C. Olivares-Galvan, J. L. Hernandez-Avila, R. Escarela-Perez, V. M. Jimenez-Mondragon, and F. Gonzalez-Montañez, "Past, present, and future of new applications in utilization of eddy currents," *Technologies*, vol. 12, no. 4, Art. no. 50, Apr. 2024, doi: 10.3390/technologies12040050.

[14]   N. M. Faudzi *et al.*, "Comparative study of ferrite and amorphous shielding materials for NFC tag antenna on metal," in *2023 IEEE International Symposium on Antennas and Propagation (ISAP)*, 2023, pp. 1–2, doi: 10.1109/ISAP57493.2023.10388437.

[15]   B. Lee, B. Kim, and S. Yang, "Enhanced loop structure of NFC antenna for mobile handset applications," *International Journal of Antennas and Propagation*, vol. 2014, pp. 1–6, 2014, doi: 10.1155/2014/187029.

[16]   B. Lee and F. J. Harackiewicz, "Design of a simple structured NFC loop antenna for mobile phones applications," *Progress in Electromagnetics Research C*, vol. 76, pp. 149–157, 2017, doi: 10.2528/PIERC17060505.

[17]   J.-Q. Zhu, Y.-L. Ban, C.-Y.-D. Sim, and G. Wu, "NFC antenna with nonuniform meandering line and partial coverage ferrite sheet for metal cover smartphone applications," *IEEE Transactions on Antennas and Propagation*, vol. 65, no. 6, pp. 2827–2835, Jun. 2017, doi: 10.1109/TAP.2017.2690532.

[18]   J. Victoria, A. Suarez, P. A. Martinez, A. Alcarria, A. Gerfer, and J. Torres, "Improving the efficiency of NFC systems through optimizing the sintered ferrite sheet thickness selection," *IEEE Transactions on Electromagnetic Compatibility*, vol. 62, no. 4, pp. 1504–1514, Aug. 2020, doi: 10.1109/TEMC.2020.3003800.

[19]   M. Bouklachi, "Design and evaluation of NFC flexible coils for communication and wireless power supply of medical monitoring patches and implants," (in French), Theses, Université Paris-Saclay, 2022.

[20]   M. E. Rahman, M. Abdelatti, M. S. Sodhi, and K. Mankodiya, "Design and performance analysis of a chemically-etched flexible NFC tag antenna," *arXiv preprint arXiv:2210.12327*, 2022.

[21]   N. A. Choudhry, L. Arnold, A. Rasheed, I. A. Khan, and L. Wang, "Textronics—a review of textile-based wearable electronics," *Advanced Engineering Materials*, vol. 23, no. 12, 2021, doi: 10.1002/adem.202100469.

[22]   K. D'hoe *et al.*, "Influence of different types of metal plates on a high frequency RFID loop antenna: study and design," *Advances in Electrical and Computer Engineering*, vol. 9, no. 2, pp. 3–8, 2009, doi: 10.4316/aece.2009.02001.

[23]   M. H. Kang, G. J. Lee, J. H. Yun, and Y. M. Song, "NFC-based wearable optoelectronics working with smartphone application

for untact healthcare," *Sensors*, vol. 21, no. 3, Jan. 2021, doi: 10.3390/s21030878.

[24] M. Gebhart, R. Neubauer, M. Stark, and D. Warnez, "Design of 13.56 MHz smartcard stickers with ferrite for payment and authentication," in *2011 Third International Workshop on Near Field Communication*, 2011, pp. 59–64, doi: 10.1109/NFC.2011.14.

[25] K. S. Rana and D. S. Ajij, "Design and simulation of NFC printed antenna in near field wireless communication for SDC," in *2016 IEEE Distributed Computing, VLSI, Electrical Circuits and Robotics (DISCOVER)*, Aug. 2016, pp. 247–251, doi: 10.1109/DISCOVER.2016.7806249.

[26] M. S. Rana *et al.*, "A review of 2.45 GHz microstrip patch antennas for wireless applications," *International Journal of Advances in Applied Sciences*, vol. 13, no. 2, Jun. 2024, doi: 10.11591/ijaas.v13.i2.pp269-281.

[27] D. Paret, *Conception d'antennes pour dispositifs NFC*. London: ISTE Group, 2015.

BIOGRAPHIES OF AUTHORS

Claude Daniel Assamoi obtained in 2015 a master's degree in physics, option electronics and telecommunication systems, at Felix Houphouët Boigny University, Abidjan, Côte d'Ivoire. He is carrying out a thesis in the technology laboratory of the physics department of the UFR SSMT of the Felix Houphouët BOIGNY University. His research focuses on the study and design of antennas in the context of the use of NFC tags in the transport sector. He can be contacted by email: assamoidaniel@gmail.com.

Yelakan Berenger Ouattara is an assistant professor in the Department of Science and Technology at Felix Houphouët Boigny University in Abidjan. He was the manager of the ICT for Forest Protection project in partnership with SODEFOR and head of the IoT/connected objects/RFID team. He holds a master's degree in HF telecommunication systems from Gustave EIFFEL (Ex. Paris-Est Marne-la-Vallee University) then a doctorate in electronics and telecommunications systems from the University of Paris-Est Sud (France). His research focuses on themes related to GNSS electronics, NFC-RFID communication, and electromagnetic phenomena. He can be contacted by email: yelouattara@gmail.com.

Bi Tra Jean Claude Youan obtained a bachelor's degree in physics and then a master's degree in electrical and electronic systems at the University Felix Houphouët Boigny in 2010 and 2013. He went on to complete a master's degree in electronics and telecommunications systems in 2015, followed by a unique doctoral thesis on improving GPS localization in constrained environments: the case of ultra-wide band technology (ULB) in 2021. Since November 2021, he has been a teacher-researcher at the University Felix Houphouët Boigny, Côte d'Ivoire. He can be contacted by email: cyouantra@gmail.com.

N'tcho Assoukpou Jean Gnamele has held, since 2023, a doctorate in physics with a specialty in networks and telecommunications from Felix Houphouët Boigny University, Côte d'Ivoire. His research work, within the technology laboratory of the physics department of the UFR SSMT, focuses on the processing of acoustic signals applied to machine learning. His work also focuses on the study of the transmission of radio signals in complex environments such as forests. He can be contacted at jeangnamele@gmail.com.

Vafi Doumbia was a 3rd cycle doctor in 1995 and a state Doctor of Physical Sciences in 2008 in geophysics, specialty "Study of the magnetic effects of the electrojet equatorial", representative of this discipline at SCOSTEP. Today, professor at Felix Houphouet-Boigny University in Abidjan, lecturer in electromagnetism, supervision of Theses. He can be contacted by email: vafid@yahoo.fr.